Available online at www.sciencedirect.com

SciVerse ScienceDirect

Journal of the European Ceramic Society 32 (2012) 1949–1956

www.elsevier.com/locate/jeurceramsoc

Influences of metallic Co and mechanical alloying on the microstructural and mechanical properties of TiB_2 ceramics prepared via pressureless sintering

Duygu Ağaoğulları *, Hasan Gökçe, İsmail Duman, M. Lütfi Öveçoğlu

Istanbul Technical University, Faculty of Chemical and Metallurgical Engineering, Department of Metallurgical and Materials Engineering, 34469 Maslak, Istanbul, Turkey

Available online 21 November 2011

Abstract

This study reports the influences of metallic cobalt (Co) and mechanical alloying (MA) on the microstructural and mechanical properties of TiB_2 ceramics prepared by using a combined method of cold pressing and sintering. The effects of Co addition (0, 5, 10 and 20 wt.%) and mechanical alloying duration (0, 3, 6 and 9 h) on the properties of TiB_2 ceramics were investigated. MA experiments were carried out in a Spex™ 8000D Mixer/Mill and milled powders were subsequently compacted to cylindrical preforms by uniaxial pressing at 400 MPa. The green compacts were sintered in a controlled atmosphere at 1550 °C for 1 h. Phase and microstructural characterizations of the mechanically alloyed (MA'd) and sintered samples were performed by X-ray diffractometer (XRD), optical microscope (OM) and scanning electron microscope (SEM). Density measurements were conducted using Archimedes method. Vickers hardness, elastic modulus and fracture toughness of the sintered samples were measured using Indentation technique.

Keywords: Milling; Pressing; Sintering; Titanium diboride; Cobalt

1. Introduction

Amongst various transition metal borides, titanium diboride (TiB_2) has attracted considerable interest due to its superior properties. With its high melting point (3225 °C), low density (4.52 g/cm^3), high hardness (25–32 GPa), high elastic modulus (565 GPa), low thermal expansion coefficient (7.4×10^{-6} K^{-1} at room temperature; 9.8×10^{-6} K^{-1} at 2000 °C), high electrical (22×10^6 Ωcm) and thermal conductivity (96 W/m/K), high wear, corrosion and thermal shock resistance, good oxidation resistance (up to 1500 °C), excellent chemical inertness and durability (to molten metals of Fe, Cu, Zn, Cd, Al, Pb, and Mg, cryolite and non-basic slags), TiB_2 has been used in a wide range of specialized applications as an advanced ceramic material.[1–5] It has been used in cutting tools, crucibles and dies for molten metals, thermocouple sheaths, ballistic armours, wear resistant coatings, electrodischarge machining electrodes and particulate reinforced composites.[5–8] TiB_2 plays important roles in aluminum industry as cathodes for the electrolytic production of aluminum due to its excellent wettability and corrosion resistance and as grain refiner in aluminum castings and in evaporation boats for the continuous evaporation of aluminum for vacuum metallization.[1,6–10] Also, it is an emerging material for integrated circuits, leading edges and nosecaps for hypersonic atmospheric re-entry, rocket nozzle inserts and high temperature nuclear reactors.[5–10]

However, consolidation problems, weak fracture toughness, flexural strength and intrinsic brittle character of TiB_2 usually restrict its extensive applications as structural material. The densification of TiB_2 requires extremely high sintering temperatures up to ~2100 °C and long dwell times because of a rather-low self diffusion coefficient caused by the predominant covalent bonding.[3,11,12] Such extreme processing conditions induces excessive grain growth, internal stresses and microcracks which are detrimental to mechanical properties.[11–14] Densification of TiB_2 is feasible at lower temperatures with the use of metallic sinter additives such as Fe, Ni, Cr, Co, Mo and Cu.[3,13,15–19] Many attempts have been made to improve the sinterability and mechanical properties of TiB_2 by adding non-metallic secondary phases, oxides (ZrO_2, Al_2O_3), carbides (SiC, B_4C, TaC, WC, TiC), nitrides (AlN, Si_3N_4, TaN, TiN, ZrN), borides (CrB_2, ZrB_2, NiB) and silicides ($MoSi_2$, $TiSi_2$).[3,11–15,20–27] A survey

* Corresponding author. Tel.: +90 212 285 6893; fax: +90 212 285 3427.
E-mail addresses: bozkurtdu@itu.edu.tr (D. Ağaoğulları), gokceh@itu.edu.tr (H. Gökçe), iduman@itu.edu.tr (İ. Duman), ovecoglu@itu.edu.tr (M.L. Öveçoğlu).

0955-2219/$ – see front matter © 2011 Elsevier Ltd. All rights reserved.
doi:10.1016/j.jeurceramsoc.2011.10.033

of the literature reveals that fully dense TiB_2 has been fabricated by hot pressing at the temperatures between 1700 and 1900 °C.[3,13,16] Although hot pressing is an effective densification process and is the major fabrication route for dense bodies, it is relatively expensive and prevents the production of complex shapes. Conversely, pressureless sintering is a cheaper method for the net-shaped products.[3,13,16]

On the basis of the reported literature, pressureless sintering of TiB_2 with Co metallic additive is not a well-discussed topic. This study presents the influence of Co additive on the microstructural and mechanical properties of TiB_2 ceramics prepared by using a combined method of mechanical alloying, cold pressing and sintering. The effects of Co addition (0, 5, 10 and 20 wt.%) and mechanical alloying duration (0, 3, 6 and 9 h) on the properties of TiB_2 ceramics were investigated.

2. Experimental procedure

Commercially available TiB_2 powders (Alfa Aesar™, 99.5% purity, <44 μm average particle size) were used as the starting material. Co powders (Eurotungstene™, >99.7% purity, 28 μm average particle size) were added to the TiB_2 powders in various amounts as the sintering additive. At each run, powder batches of 10 g were weighed in a Precisa™ XB320M sensitive balance (precision: 0.001 g). The powders were mixed to constitute the blends in the compositions of TiB_2–5 wt.% Co (9.5 g TiB_2), TiB_2–10 wt.% Co (9.0 g TiB_2) and TiB_2–20 wt.% Co (8.0 g TiB_2). Mechanical alloying (MA) experiments were carried out using a Spex™ 8000 D Mixer/Mill with a rotation speed of 1200 rpm in a tungsten carbide (WC) vial (50 ml) with WC balls (Ø 6.5 mm). Before MA, powder blends were placed into the milling vials and the vials were evacuated to about 10^{-2} Pa and sealed in a Plaslabs™ glove box under Ar gas (Linde™, 99.999% purity) to prevent surface oxidation and contamination of powder particles. MA experiments were carried out using a 10:1 ball-to-powder weight ratio (BPR) for 3, 6 and 9 h durations. Mechanically alloyed (MA'd) powders were unloaded again under Ar atmosphere in the glove-box at the end of mentioned durations. Non-MA'd (as-blended) powders were mixed in a WAB™ T2C Turbula blender for 4 h. All as-blended and MA'd powders were compacted in a 10 ton capacity MSE™ MP-0710 uni-action hydraulic press to obtain cylindrical preforms with a diameter of 12.7 mm under an uniaxial pressure of 400 MPa. The green bodies were sintered at 1550 °C for 1 h in a Linn™ HT-1800 high temperature controlled atmosphere furnace with a heating and cooling rate of 8 °C/min, under vacuum up to 400 °C and under Ar gas flowing conditions between 400 and 1550 °C.

The phase compositions of the as-blended powders, MA'd powders and sintered samples were performed by X-ray diffraction (XRD) technique using a Bruker™ D8 Advanced Series Powder Diffractometer with CuKα ($\lambda = 1.5406$ Å) radiation in the 2θ range of 20–80° incremented at a step size of 0.02° at a rate of 2°/min. International Center for Diffraction Data® (ICDD) powder diffraction files were utilized for the identification of crystalline phases. The average crystallite sizes of the MA'd powders were determined using a Bruker™-AXS TOPAS V3.0 software.[28] To determine the repeatability of the crystal size measurements, the same XRD investigations were carried out two times per each powder blend MA'd for different durations by changing the scan rate as 1°/min and 2°/min. Densities of the sintered samples were determined by Archimedes method using ethanol and the results were reported as the arithmetic means of three different measurements taken from the same samples. In order to obtain scratch-free mirror finish in microstructure and microhardness specimens, sintered samples were hot-mounted in Struers™ Labopress1, grounded with a diamond wheel and polished with diamond slurries in Buehler™ EcomedII and cleaned ultrasonically (Bandelin™ Sonorex) in isopropyl alcohol for 10 min. Microstructures and energy dispersive spectroscopy (EDS) analyses of the sintered samples were observed by using Nikon™ Eclipse L150 optical microscope (OM) screened by Clemex Vision Lite image analysis software and Jeol™ JSM 7000F field emission scanning electron microscope (FE-SEM) operated at 15 kV. EDS results were reported as the arithmetic means of three different measurements taken from the same regions in the samples. Vickers microhardnesses of the sintered samples were measured using a Shimadzu™ HMV Microhardness Tester under a load of 2.942 N for 15 s. Microhardness test result for each sample includes the arithmetic mean of twelve successive indentations and standard deviations. For further understanding of the mechanical behaviour, depth sensing indentation measurements were performed at a peak load of 3 N, using a CSM™ International MHT SN 06-0212 instrumented Vickers indenter. The load versus penetration depth curves were obtained at a loading and unloading rate of 0.1 N/s with a holding time of 10 s at the peak loads. The fracture toughness were determined by crack length measurement of the radial crack pattern formed around Vickers indents which was applied by Zwick™ ZHU 2.5 at loads of 100, 200 and 500 N for 5 s.

3. Results and discussion

Fig. 1(a) and (b) illustrates the XRD patterns of the TiB_2–10 wt.% Co and TiB_2–20 wt.% Co powder blends MA'd for different durations, respectively. It is seen from Fig. 1(a) and (b) that there is no reaction between TiB_2 and Co particles after milling for 3, 6 and 9 h because TiB_2 (ICDD Card No: 35-0741, Bravais lattice: primitive hexagonal, $a = b = 0.303$ nm, $c = 0.323$ nm) phase is present in the powder blends without any additional phase. Very weak Co (ICDD Card No: 89-4308, Bravais lattice: primitive hexagonal, $a = b = 0.250$ nm, $c = 0.409$ nm) reflections are observed only in the XRD patterns of the TiB_2–20 wt.% Co powder blends (Fig. 1(b)). For the TiB_2–10 wt.% Co powder blends, Co peaks are suppressed and cannot be detected because of negative X-ray beam interference by the CuKα radiation source. Because of this, XRD patterns of the TiB_2–5 wt.% Co powder blends MA'd for different durations are not shown in Fig. 1. Also, XRD patterns of the TiB_2–0 wt.% Co powder blends MA'd for different durations were not included into Fig. 1 since they only contains TiB_2 phase. As seen in Fig. 1(a) and (b), TiB_2 peaks gradually decreased in

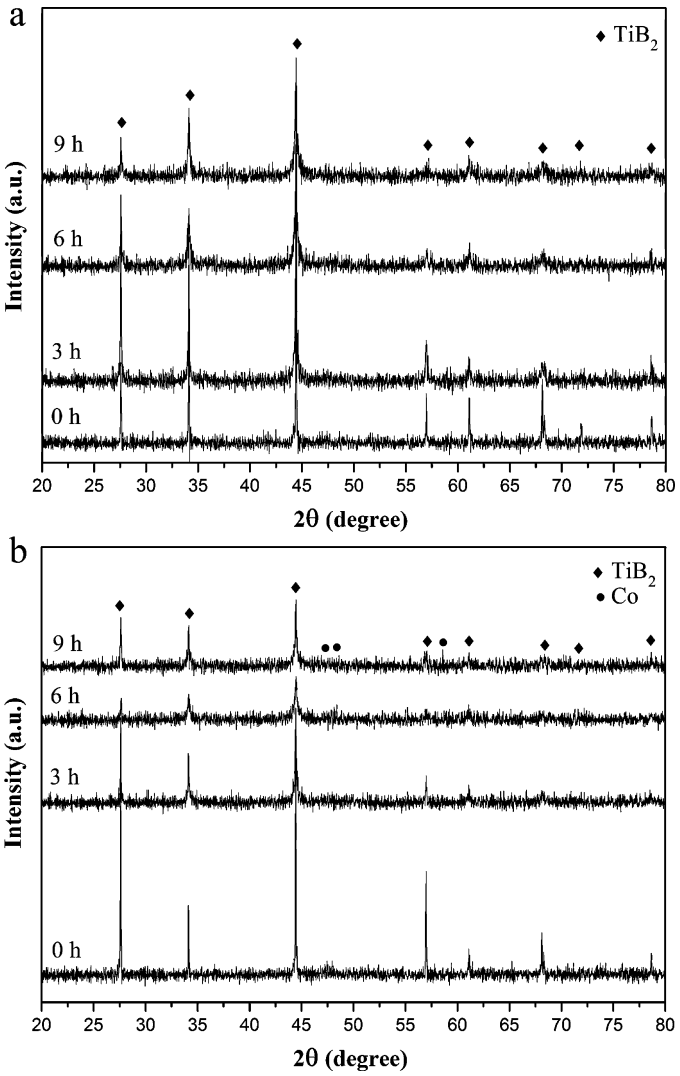

Fig. 1. XRD patterns of the TiB_2–x wt.% Co powder blends (x = 10 and 20) MA'd for different durations: (a) TiB_2–10 wt.% Co and (b) TiB_2–20 wt.% Co.

intensity and broadened with increasing milling duration (from 0 to 9 h). Continuous deformation of powder particles during milling results in crystallite refinement and increase in lattice strain. The average crystallite sizes of TiB_2 in the TiB_2–x wt.% Co powder blends (x = 0, 5, 10 and 20) MA'd for different durations are given in Table 1. These values were calculated from the arithmetic mean of three reflection measurements indexed to (0 1 0), (0 0 1) and (0 1 1) crystal planes taken from two different XRD patterns at different scan rates. Average crystallite sizes of all compositions decrease as milling duration increases from 0 to 9 h. The declines in the amount of crystallite refinement are much sharper between the blends MA'd for 0 and 3 h than those between 3 and 9 h. After MA reaches a steady-state condition at the milling duration of 6 h, a significant reduction in average crystallite sizes no longer occurs and a maximum crystallite size difference of 3 nm between 6 and 9 h becomes evident.

Fig. 2(a)–(c) shows the XRD patterns of the TiB_2–5 wt.% Co, TiB_2–10 wt.% Co and TiB_2–20 wt.% Co samples MA'd for different durations and sintered at 1550 °C for 1 h, respectively. As seen in the XRD patterns in Fig. 2(a), sintered

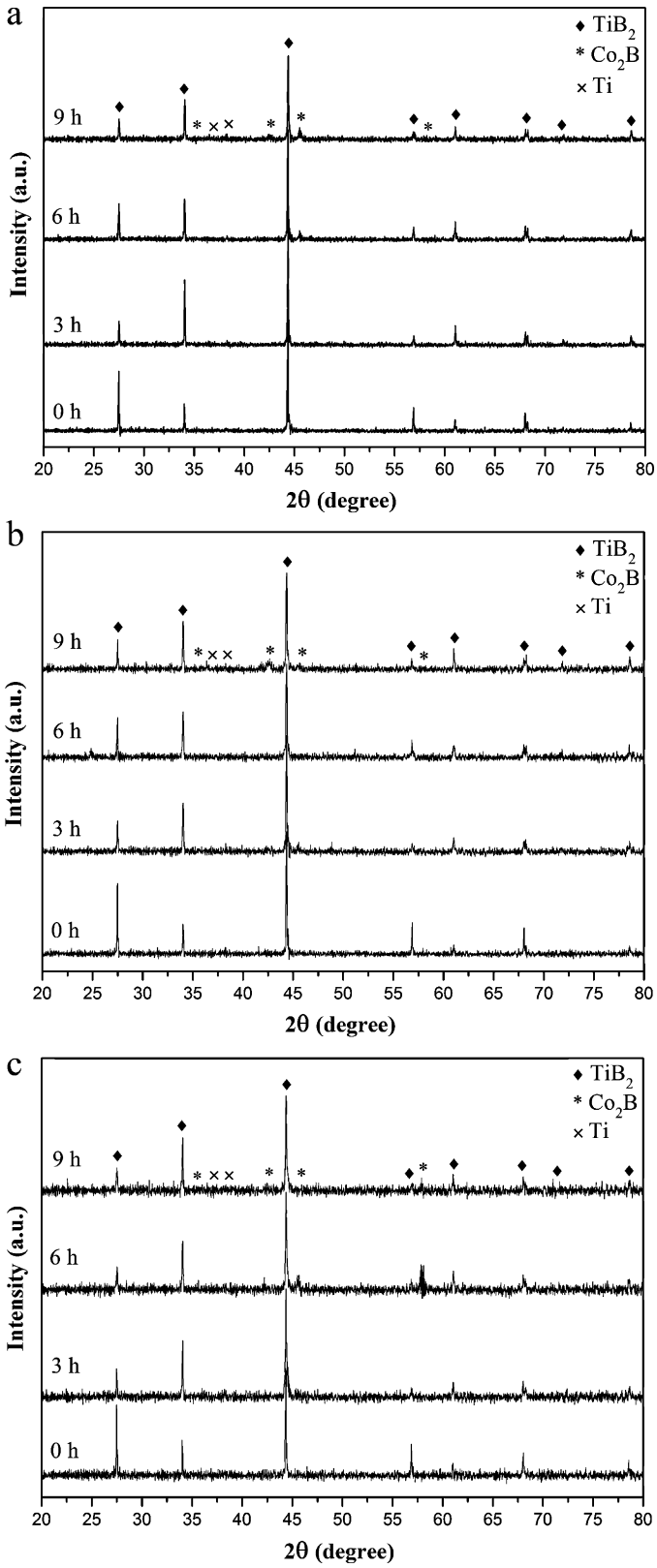

Fig. 2. XRD patterns of the sintered TiB_2–x wt.% Co samples (x = 0, 5, 10 and 20) MA'd for different durations: (a) TiB_2–5 wt.% Co, (b) TiB_2–10 wt.% Co and (c) TiB_2–20 wt.% Co.

Table 1
The average crystallite sizes of TiB_2 in the TiB_2–x wt.% Co powder blends (x = 0, 5, 10 and 20) MA'd for different durations.

Sample composition	MA duration (h)	Average crystallite size (nm)
TiB_2–0Co	0	922 ± 46
TiB_2–0Co	3	47 ± 6
TiB_2–0Co	6	36 ± 5
TiB_2–0Co	9	34 ± 2
TiB_2–5Co	0	914 ± 38
TiB_2–5Co	3	51 ± 9
TiB_2–5Co	6	41 ± 7
TiB_2–5Co	9	39 ± 2
TiB_2–10Co	0	782 ± 37
TiB_2–10Co	3	93 ± 5
TiB_2–10Co	6	50 ± 3
TiB_2–10Co	9	49 ± 2
TiB_2–20Co	0	761 ± 33
TiB_2–20Co	3	103 ± 8
TiB_2–20Co	6	90 ± 4
TiB_2–20Co	9	87 ± 3

Table 2
Density measurements of the sintered TiB_2–x wt.% Co samples (x = 0, 5, 10 and 20) MA'd for different durations.

Sample composition	MA duration (h)	$\rho_{theoretical}$ (g/cm^3)	$\rho_{relative}$ (%)
TiB_2–0Co	0	4.52	51.2
TiB_2–0Co	3		72.9
TiB_2–0Co	6		73.4
TiB_2–0Co	9		68.2
TiB_2–5Co	0	4.63	67.9
TiB_2–5Co	3		94.9
TiB_2–5Co	6		96.2
TiB_2–5Co	9		92.5
TiB_2–10Co	0	4.75	68.6
TiB_2–10Co	3		95.0
TiB_2–10Co	6		96.9
TiB_2–10Co	9		92.8
TiB_2–20Co	0	5.01	69.3
TiB_2–20Co	3		96.8
TiB_2–20Co	6		97.6
TiB_2–20Co	9		93.3

TiB_2–5 wt.% Co samples prepared from as-blended powders and those MA'd for 3 h have TiB_2 and very small amount of Ti (ICDD Card No: 44-1294, Bravais lattice: primitive hexagonal, $a = b = 0.295$ nm, $c = 0.468$ nm) phases. TiB_2, Ti and Co_2B (ICDD Card No: 25-0241, Bravais lattice: body-centered tetragonal, $a = b = 0.502$ nm, $c = 0.422$ nm) phases are present in the same sample MA'd for 6 and 9 h. Formation of Co_2B arises from the dissolution of TiB_2 in the liquid cobalt at the sintering temperature of 1550 °C which is higher than the melting point of Co (T_m = 1495 °C). Thus, elemental Ti and Co_2B were detected together in fewer amounts in the XRD patterns of the sintered TiB_2–5 wt.% Co MA'd for 6 and 9 h. It has been also reported in the current literature that transition metals react with TiB_2 to form metallic borides of the MB, M_2B and $M_{23}B_6$ types.[17] Additionally, the intensities of Ti and Co_2B peaks are somewhat higher for the 9 h MA'd sample than that of the 6 h MA'd sample because MA increases the possibility of the TiB_2 dissolution and Co-B reaction. As clearly seen from Fig. 2(b), Co_2B phase occurs in the sintered TiB_2–10 wt.% Co sample after MA for 3 h. Moreover, very small Co_2B incubation is observed in the non-MA'd and sintered TiB_2–20 wt.% Co sample (Fig. 2(c)). This means that the solubility of TiB_2 increases with the cobalt content in the composition and hence the cobalt activity in the liquid increases. Conversely, if the Co additive content is kept constant, MA accelerates the formation of the Co_2B phase.

Density measurements of the sintered TiB_2–x wt.% Co samples (x = 0, 5, 10 and 20) MA'd for different durations are shown in Table 2. High density values for the sintered pure TiB_2 are almost impossible to be achieved due to its high melting point and low bulk diffusivity, using either pressureless sintering or hot-pressing techniques. Thus, sintered TiB_2–0 wt.% Co sample prepared from as-blended powders has the lowest relative density value of 51.2%. Densification can be enhanced with small additions of metallic additives to form the liquid phase.[13,15,16] It is strikingly evident from Table 2 that both the presence of metallic Co and MA have positive contributions on the relative density values of sintered samples. For all sintered as-blended samples in which the effect of Co is considered alone, the relative density values increase by 17–18% from that of the sample containing no Co (TiB_2–0 wt.% Co). However, the highest relative density value for the sintered as-blended samples is only 69.3% measured for the TiB_2–20 wt.% Co sample. This value is extremely low indicating that a relatively high content of metallic Co has had an inadequate effect on the densification. This can be attributed to inhomogeneous distribution of Co in the as-blended powders resulting in segregation, poor or no wetting between TiB_2 and Co particles during sintering.

When the effects of Co content and MA are considered together, namely for the MA'd Co containing samples, the density values are 92.5% and above (Table 2). For the constant MA duration, it can be easily seen from Table 2 that the relative densities of the sintered samples increase by about 24% from the sample containing no Co to those containing various amounts of Co. This indicates that a liquid phase and increase in its amount can improve the densification rate. Moreover, extending milling times up to 6 h have a positive effect on the densities when the cobalt content is fixed. This effect is more remarkable in the sintered samples which were prepared from as-blended powders and those MA'd for 3 h. Furthermore, it is completely supported by the sharp difference in the average crystallite sizes of these samples since the smaller crystallites result in higher densification rates. As the cobalt content is fixed, it is easily distinguished that the MA duration of 9 h have a negative effect on the density values because of the increase in the fraction of Co_2B phase. The highest relative density was obtained as 97.6% in the sintered TiB_2–20 wt.% Co sample MA'd for 6 h. However, the use of metallic additives have demonstrated that an approximately 99% relative density can be achieved via liquid phase sintering.[13,16,26] TiB_2 ceramics with a relative density of 98.8% can be obtained by pressureless sintering at 1900 °C with the simultaneous addition of classical sintering aids such

Table 3
Microhardness measurements of the sintered TiB_2–x wt.% Co samples (x = 5, 10 and 20) MA'd for different durations.

Sample composition	MA duration (h)	$HV_{0.3}$ (GPa)
TiB_2–5Co	0	–
TiB_2–5Co	3	24.90 ± 0.20
TiB_2–5Co	6	30.29 ± 0.17
TiB_2–5Co	9	24.77 ± 0.11
TiB_2–10Co	0	–
TiB_2–10Co	3	21.80 ± 0.25
TiB_2–10Co	6	26.40 ± 0.32
TiB_2–10Co	9	18.46 ± 0.40
TiB_2–20Co	0	–
TiB_2–20Co	3	19.03 ± 0.18
TiB_2–20Co	6	22.77 ± 0.51
TiB_2–20Co	9	18.24 ± 0.15

as Fe and Cr, which the high density value is attributed to the Ti–Fe–Cr phase existed at the triple junction.[16] In the present study, it should be noted that if the sintering temperatures above 1550 °C are employed, higher relative density values might be achieved considering the contributions of both Co content and MA.

Microhardness measurements of the sintered TiB_2–x wt.% Co samples (x = 5, 10 and 20) MA'd for different durations are given in Table 3. Vickers indents cannot be applied to the non-MA'd and sintered TiB_2–5 wt.% Co, TiB_2–10 wt.% Co and TiB_2–20 wt.% Co samples due to their analogous microstructures presented in Fig. 3(a). Indentations could not be taken from all sintered TiB_2–0 wt.% Co samples as a result of inadequate sintering conditions in which 1550 °C is lower than the sintering temperature of pure TiB_2. On the basis of Table 3, MA'd TiB_2–5 wt.% Co samples have the highest microhardness values compared to those of the TiB_2–10 wt.% Co and TiB_2–20 wt.% Co. Amongst them, a maximum hardness value (30.29 ± 0.17 GPa) was measured in the TiB_2–5 wt.% Co sample MA'd for 6 h. Fig. 3(b)–(d) shows the OM images of the sintered TiB_2–x wt.% Co (x = 5, 10 and 20) samples MA'd for 6 h. As the Co content increases from 5 to 20 wt.% at the constant MA duration, hardness gradually decreases from 24.90 ± 0.20 to 18.24 ± 0.15 GPa. Besides, microhardness values increase with increasing MA duration up to 6 h, for the same Co contents. MA durations exceeding 6 h have negative effects on the hardness values similar with the density measurements presented in Table 2. Therefore, both milling for 9 h and increasing Co content cause an increase in the fraction of Co_2B phase, which it decreases the hardness.

Oliver and Pharr methodology was followed for the determination of the elastic modulus. Reduced elastic modulus (E^*) can be estimated according to the elastic theory given in Eq. (1), where $A(\delta)$ is the contact area at maximum penetration and $dP/d\delta$ is the derivative of the experimental curve taken at the load peak along the unloading path.[29–31] Fig. 4(a)–(c) shows the load versus penetration depth curves of the MA'd for 6 h and sintered TiB_2–5 wt.% Co, TiB_2–10 wt.% Co and TiB_2–20 wt.% Co samples, respectively.

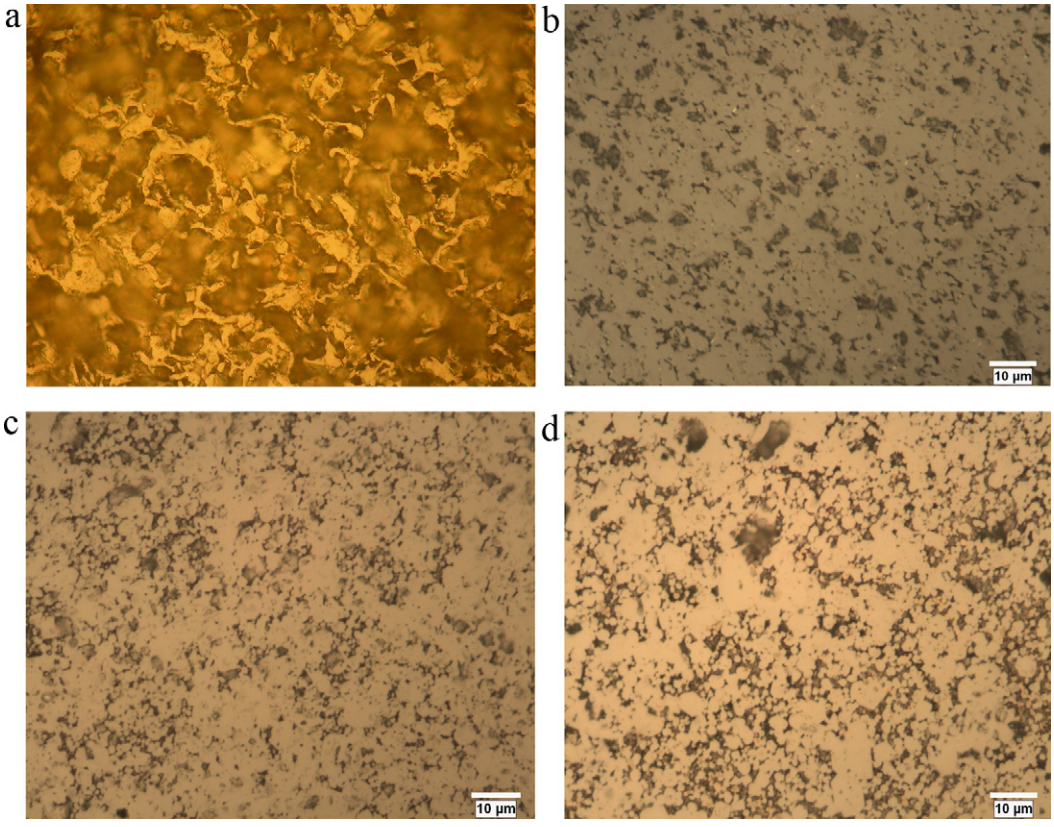

Fig. 3. OM images of the sintered samples: (a) analogous microstructures of TiB_2–x wt.% Co (x = 5, 10 and 20) MA'd for 0 h, (b) TiB_2–5 wt.% Co MA'd for 6 h, (c) TiB_2–10 wt.% Co MA'd for 6 h and (d) TiB_2–20 wt.% Co MA'd for 6 h.

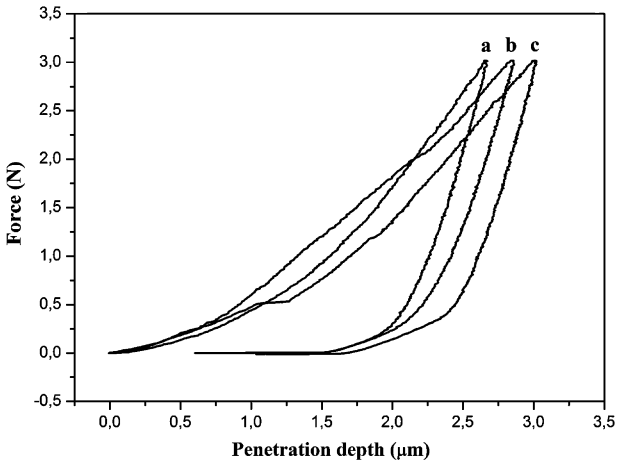

Fig. 4. The load versus penetration depth curves of the sintered samples MA'd for 6 h: (a) TiB_2–5 wt.% Co, (b) TiB_2–10 wt.% Co and (c) TiB_2–20 wt.% Co.

Unknown elastic modulus of the samples can be calculated by using Eqs. (1) and (2) when Poisson's ratio for the TiB_2-based ceramics (υ_{sample}) is assumed as 0.2 and Poisson's ratio (υ_{tip}) and elastic modulus (E_{tip}) of the diamond tip are taken as 0.07 and 1141 GPa.[12,32]

$$E* = -\frac{1}{2}\frac{dP}{d\delta}\sqrt{\frac{\pi}{A(\delta)}} \quad (1)$$

$$\frac{1}{E*} = \frac{1-\upsilon_{tip}^2}{E_{tip}} + \frac{1-\upsilon_{sample}^2}{E_{sample}} \quad (2)$$

In regard of Eq. (1) and (2), the elastic modulus of the MA'd for 6 h and sintered TiB_2–5 wt.% Co, TiB_2–10 wt.% Co and TiB_2–20 wt.% Co samples were found as 514 ± 15 GPa, 485 ± 7 GPa and 457 ± 18 GPa. Similar to the hardness results in Table 3, the highest elastic modulus was obtained in the TiB_2–5 wt.% Co sample and E values decrease gradually as cobalt content increases. The calculated values of elastic modulus have the same tendency with different type of additives in the reported literature: The increase in weight percentages of $MoSi_2$, $TiSi_2$ and AlN additives in TiB_2 ceramics decreases the elastic modulus.[11,12,14,24,26,27] Due to the fact that the sintered TiB_2–5 wt.% Co MA'd for 6 h has the best results, fracture toughness tests were conducted on this sample (Fig. 5). No propagation of indentation cracks was observed even under both loads of 100 (Fig. 5(a)) and 200 N (Fig. 5(b)). Absence of crack propagation is compatible with high elastic modulus values measured for the sintered TiB_2–5 wt.% Co sample MA'd for 6 h. Dissimilar to the current literature[12,14] in which TiB_2-based ceramics were subjected to the fracture toughness measurements, a 500 N load was also applied to the sintered TiB_2–5 wt.% Co sample MA'd for 6 h (Fig. 5(c)). Since the crack line does not appear to be fairly straight and radial cracks do not emanate from the four indentation corners (Fig. 5(c)), it is hard to calculate the fracture toughness value correctly.

Fig. 6(a) is the SEM image of the non-MA'd and sintered TiB_2–0 wt.% Co sample. As seen in this figure, microstructure consists of irregular particles ranging in size between 900 nm and 10 μm. Fig. 6(b) illustrates the SEM image of the

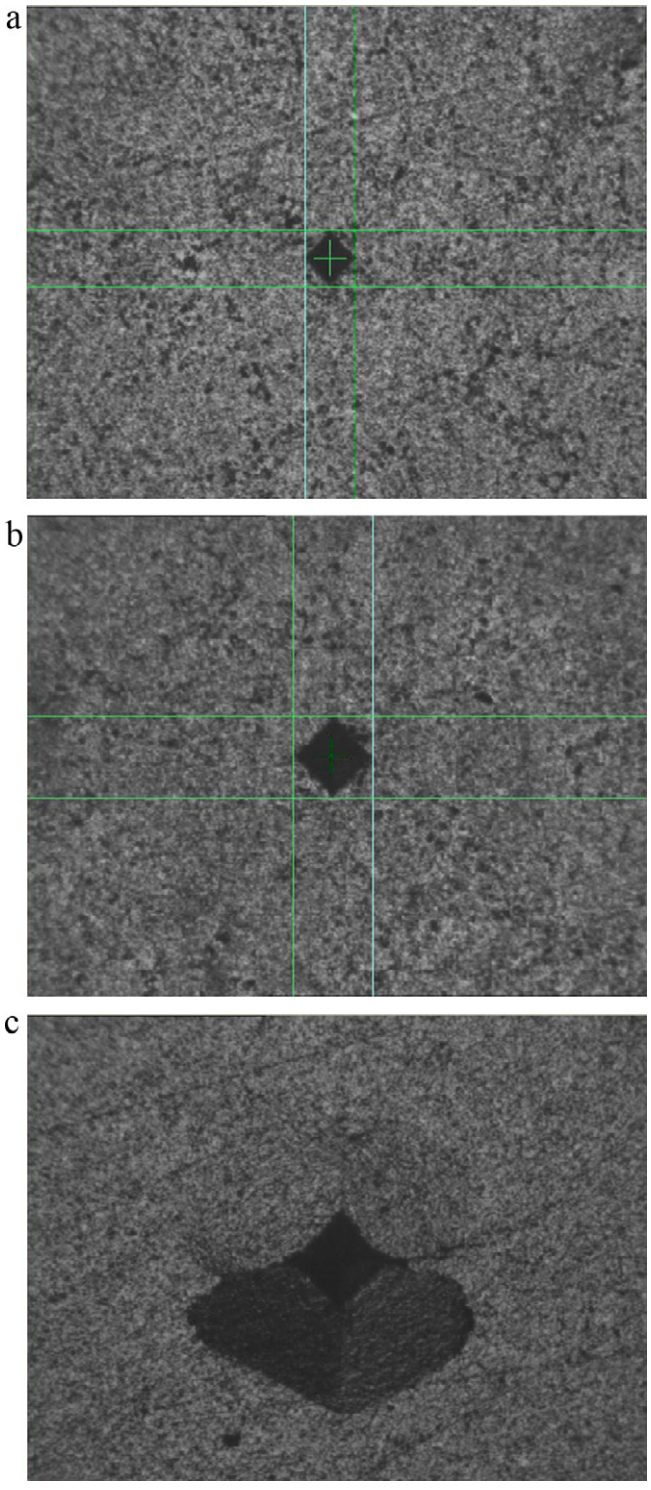

Fig. 5. Vickers indentations conducted on the sintered TiB_2–5 wt.% Co sample MA'd for 6 h: (a) at a load of 100 N, (b) 200 N and (c) 500 N.

non-MA'd and sintered TiB_2–5 wt.% Co sample. As compared with Fig. 6(b), the non-MA'd and sintered TiB_2–0 wt.% Co sample in Fig. 6(a) exhibits low densification rate which is in accordance with the inadequate sintering conditions and lowest relative density value (Table 2). It is obvious from Fig. 6(a) and (b) that 5 wt.% Co addition somewhat increases the densification even if MA is not conducted on the powder blends

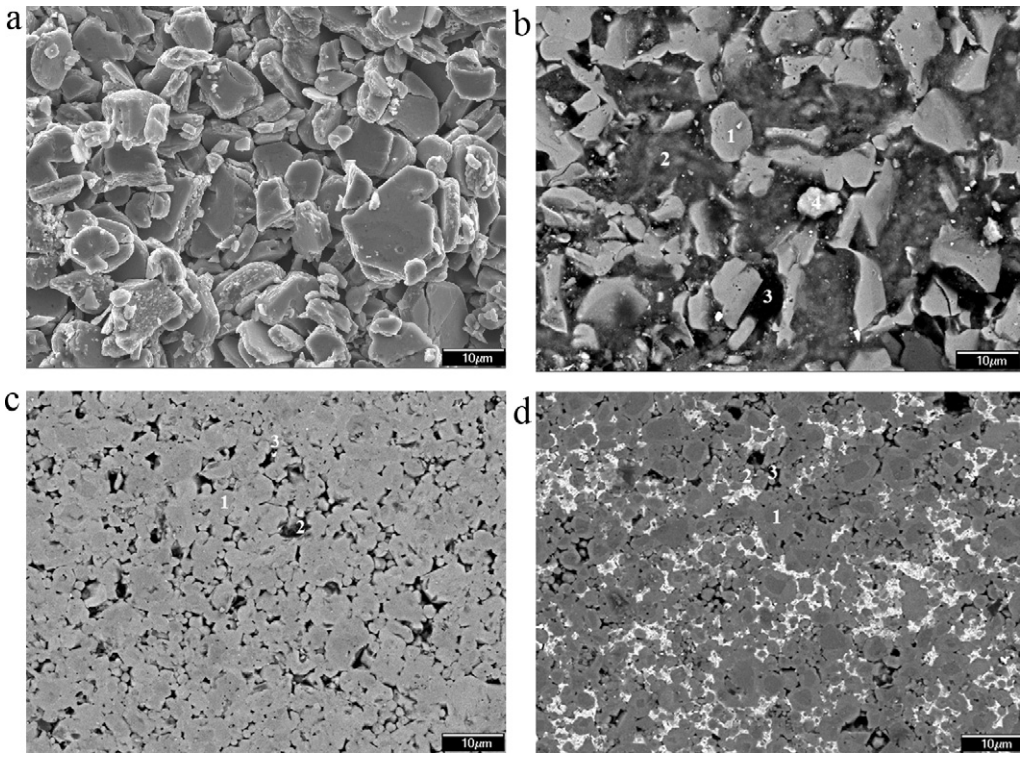

Fig. 6. SEM images of the sintered TiB_2–x wt.% Co samples (x = 0, 5 and 20) MA'd for different durations: (a) TiB_2–0 wt.% Co MA'd for 0 h, (b) TiB_2–5 wt.% Co MA'd for 0 h, (c) TiB_2–5 wt.% Co MA'd for 6 h and (d) TiB_2–20 wt.% Co MA'd for 6 h.

before sintering. On the basis of several EDS measurements taken from the mentioned regions in Fig. 6(b), region 1 shows the TiB_2 particle containing 68 ± 4 wt.% Ti and 32 ± 2 wt.% B. Region 2 and 4 indicate the Co-rich regions in the microstructure respectively involving 34 ± 5% Ti and 66 ± 2% Co and 6 ± 2% Ti and 94 ± 6% Co. On the other hand, region 3 is the Ti-rich region of the sintered body in which 82 ± 3 wt.% Ti and 18 ± 4 wt.% Co are present. Fig. 6(b) shows a more denser microstructure with the addition of 5 wt.% Co in comparison with Fig. 6(a). SEM images of the sintered TiB_2–5 wt.% Co and TiB_2–20 wt.% Co samples MA'd for 6 h are given respectively in Fig. 6(c) and (d). In Fig. 6(c), region 1 has 63 ± 7 wt.% Ti and 37 ± 3 wt.% B whereas 16 ± 2 wt.% Ti and 84 ± 5 wt.% Co are present in region 2. In addition to 34 ± 2 wt.% Ti and 16 ± 3 wt.% B, small white particles marked as region 3 involves 28 ± 4 wt.% W and 21 ± 3 wt.% C. As clearly seen from the microstructure difference between Fig. 6(b) and (c), MA provides the crystallite refinement (Table 1) and hence the homogeneous distribution of TiB_2 and Co particles throughout the sintered body. Besides, WC contamination released by the milling vial and balls was detected by the EDS analysis differing from the XRD results. Fig. 6(d) has also three different regions containing 64 ± 6 wt.% Ti and 36 ± 4 wt.% B (region 1), 5 ± 2 wt.% Ti and 95 ± 8 wt.% Co (region 2) and 70 ± 4 wt.% Ti, 3 ± 0.5 wt.% Co, 5 ± 2 wt.% W and 21 ± 5 wt.% C (region 3). Fig. 6(d) is compatible with the relative density values in Table 2 since there is a slight increase in the densification rate of TiB_2 surrounded by higher amount of Co particles.

4. Conclusions

Based on the results of the present study, the following conclusions can be drawn:

- A combined method of mechanical alloying, cold pressing and sintering is successfully utilized in the fabrication of TiB_2–x wt.% Co (x = 0, 5, 10 and 20) ceramics. Mechanical alloying provides a sharp decrease in average crystallite sizes of TiB_2.
- Co_2B formation was observed in all Co contents (5, 10 and 20 wt.%) dependent to the MA duration, after sintering at 1550 °C for 1 h. When the additive content is kept constant, MA accelerates the formation of boride phase. Prolonging milling time up to 6 h have a positive effect on the densities and hardness values when the cobalt content is fixed. However, WC contamination released by the milling vial and balls was detected in the sintered samples MA'd for 6 h.
- The relative densities of the sintered samples increase as cobalt content increases from 0 to 20 wt.%. The highest relative density was found as 97.6% in the sintered TiB_2–20 wt.% Co sample MA'd for 6 h.
- The highest microhardness and elastic modulus values were obtained in the sintered TiB_2–5 wt.% Co sample MA'd for 6 h, respectively as 30.29 ± 0.17 GPa and 514 ± 15 GPa. There is no crack propagation in the sintered TiB_2–5 wt.% Co sample MA'd for 6 h, under the loads of 100 and 200 N.

Acknowledgements

We would like to express our appreciations to Prof. Dr. Hüseyin Çimenoğlu for his help in elastic modulus and fracture toughness measurements. Further, we would like to express our gratitude to State Planning Organization (DPT) for funding the projects entitled "Advanced Technologies in Engineering" with the project number 2001K120750 and "Development of Al–Cu Based Metal Matrix Composites via Powder Metallurgy Techniques" with the project number 90189 out of which the main infrastructure of the Particulate Materials Laboratories was founded.

References

1. Weimer AW. *Carbide, nitride and boride materials synthesis and processing*. Cambridge, Great Britain: Chapman & Hall; 1997.
2. Munro RG. Material properties of titanium diboride. *J Res Natl Inst Stan* 2000;**105**:709–20.
3. Subramanian C, Murthy TSRCh, Suri AK. Synthesis and consolidation of titanium diboride. *Int J Refract Met Hard Mater* 2007;**25**:345–50.
4. Han Y, Dai Y, Shu D, Wang J, Sun B. Electronic and bonding properties of TiB_2. *J Alloys Compd* 2007;**438**:327–31.
5. Khanra AK, Godkhindi MM. Comparative studies on sintering behavior of self-propagating high-temperature synthesized ultra-fine titanium diboride powder. *J Am Ceram Soc* 2005;**88**:1619–21.
6. Ricceri R, Matteazzi P. A fast and low-cost room temperature process for TiB_2 formation by mechanosynthesis. *Mater Sci Eng A* 2004;**379**:341–6.
7. Hayk K, Suren K. Combustion synthesis of titanium diboride and zirconia composite powders: part I. *J Am Ceram Soc* 2008;**91**:3504–9.
8. Gu Y, Qian Y, Chen L, Zhou F. A mild solvothermal route to nanocrystalline titanium diboride. *J Alloys Compd* 2003;**352**:325–7.
9. Bača L', Stelzer N. Adapting of sol-gel process for preparation of TiB_2 powder from low-cost precursors. *J Eur Ceram Soc* 2008;**28**:907–11.
10. Welham NJ. Formation of TiB_2 from rutile by room temperature ball milling. *Miner Eng* 1999;**12**:1213–24.
11. Li LH, Kim HE, Kang ES. Sintering and mechanical properties of titanium diboride with aluminum nitride as a sintering aid. *J Eur Ceram Soc* 2002;**22**:973–7.
12. Mukhopadhyay A, Raju GB, Basu B, Suri AK. Correlation between phase evolution, mechanical properties and instrumented indentation response of TiB_2-based ceramics. *J Eur Ceram Soc* 2009;**29**:505–16.
13. Einarsrud MA, Hagen E, Pettersen G, Grande T. Pressureless sintering of titanium diboride with nickel, nickel boride, and iron additives. *J Am Ceram Soc* 1997;**80**:3013–20.
14. Murthy TSRCh, Sonber JK, Subramanian C, Fotedar RK, Gonal MR, Suri AK. Effect of CrB_2 addition on densification, properties and oxidation resistance of TiB_2. *Int J Refract Met Hard Mater* 2009;**27**:976–84.
15. Gu M, Huang C, Zou B, Liu B. Effect of (Ni, Mo) and TiN on the microstructure and mechanical properties of TiB_2 ceramic tool materials. *Mater Sci Eng* 2006;**433**:39–44.
16. Kang SH, Kim DJ. Pressureless sintering and properties of titanium diboride ceramics containing chromium and iron. *J Am Ceram Soc* 2001;**84**:893–5.
17. Sánchez JM, Azcona I, Castro F. Mechanical properties of titanium diboride based cermets. *J Mater Sci* 2000;**35**:9–14.
18. González R, Barandika MG, Ona D, Sánchez JM, Villellas A, Valea A, et al. New binder phases for the consolidation of TiB_2 hardmetals. *Mater Sci Eng A-Struct* 1996;**216**:185–92.
19. Suskin S, Chepovetsky GI. Comparison of vacuum and pressure-assisted sintering of TiB_2-Ni. *J Mater Eng Perform* 1996;**5**:396–8.
20. Torizuka S, Sato K, Nishio H, Kishi T. Effect of SiC on interfacial reaction and sintering mechanism of TiB_2. *J Am Ceram Soc* 1995;**78**:1606–10.
21. Kang ES, Kim CH. Improvements in mechanical properties of TiB_2 by the dispersion of B_4C particles. *J Mater Sci* 1990;**25**:580–4.
22. Kang ES, Jang CW, Lee CH, Kim CH. Effect of iron and boron carbide on the densification and mechanical properties of titanium diboride ceramics. *J Am Ceram Soc* 1989;**72**:1868–72.
23. Cobb PC. Titanium carbide as a sintering agent for titanium boride. *Mater Des* 1990;**11**:156–9.
24. Raju GB, Basu B, Tak NH, Cho SJ. Temperature dependent hardness and strength properties of TiB_2 with $TiSi_2$ sinter-aid. *J Eur Ceram Soc* 2009;**29**:2119–28.
25. Gu M, Huang C, Xiao S, Liu H. Improvements in mechanical properties of TiB_2 ceramics tool materials by the dispersion of Al_2O_3 particles. *Mater Sci Eng A-Struct* 2008;**486**:167–70.
26. Raju GB, Basu B. Influence of $MoSi_2$ addition on load-dependent fretting wear properties of TiB_2 against cemented carbide. *J Am Ceram Soc* 2009;**92**:2059–66.
27. Mukhopadhyay A, Raju GB, Basu B. Understanding influence of $MoSi_2$ addition (5 weight percent) on tribological properties of TiB_2. *Metall Mater Trans A* 2008;**39A**:2998–3013.
28. Kern AA, Coelho AA. Bruker-AXS TOPAS V.3.0, 2006, www.brukeraxs.com.
29. Oliver WC, Pharr GM. An improved technique for determining hardness and elastic modulus using load and displacement sensing indentation experiments. *J Mater Res* 1992;**7**:1564–83.
30. Pharr GM, Oliver WC, Brotzen FR. On the generality of the relationship among contact stiffness, contact area, and elastic modulus during indentation. *J Mater Res* 1992;**7**:613–7.
31. Oliver WC, Pharr GM. Measurement of hardness and elastic modulus by instrumented indentation: advances in understanding and refinements in methodology. *J Mater Res* 2004;**19**:3–20.
32. Rinaldi A, Correa-Duarte MA, Salgueirino-Maceira V, Licoccia, Traversa E, Dávila-Ibánez AB, et al. Elastic properties of hard cobalt boride composite nanoparticles. *Acta Mater* 2010;**58**:6474–86.